Anatomia, Histologia, Embryologia

WILEY

Anatomia Histologia Embryologia

ORIGINAL ARTICLE OPEN ACCESS

Conjoined Parasitic Twins (Cephalo-Thoracopagus Parasiticus) in a Free Ranging Northern Bat (*Eptesicus nilssonii*): A Micro-CT Anatomic and Genetic Survey

J. Meyer[1] | V. N. Laine[2] | J. van der Kooij[3] | B. Richter[4] | S. Handschuh[5] | M. Gumpenberger[6]

[1]Tierarztpraxis Voelkendorf, Villach, Austria | [2]Finnish Museum of Natural History, University of Helsinki, Helsinki, Finland | [3]Nature Education, Research and Consultancy Van der Kooij, Slattum, Norway | [4]Department of Biological Sciences and Pathobiology, Institute of Pathology, University of Veterinary Medicine, Vienna, Austria | [5]VetCoreFacility for Research, Imaging Unit, University of Veterinary Medicine Vienna, Vienna, Austria | [6]Diagnostic Imaging, Department for Companion Animals and Horses, University of Veterinary Medicine, Vienna, Austria

Correspondence: M. Gumpenberger (michaela.gumpenberger@vetmeduni.ac.at)

Received: 14 November 2025 | **Revised:** 14 November 2025 | **Accepted:** 9 January 2026

Keywords: chiroptera | conjoined parasitic twins | diagnostic micro-CT imaging | *Eptesicus nilssonii* | northern bat | wild animals

ABSTRACT

The detailed anatomical situation of male stillborn cephalo-thoracopagus twins in a wild ranging northern bat (*Eptesicus nilssonii*) is described by means of full body micro-CT scans in high resolution with three-dimensional computational reconstruction. The external anatomy was characterised by supernumerary wings and legs and marked cranial disfiguration. The most striking features of the internal anatomy were the presence of two hearts with different characteristics, three lungs with two tracheas, three kidneys as well as a doubled liver. Vascular aberrations and other organ deformities are described in detail. The monozygotic origin of the present parasitic conjoined twin was shown by genetic sequencing, analysis and relatedness calculations based on individual tissue samples from the autosite and the parasite. As the free ranging 1 year old mother of this twin returned every year to the same well monitored nursery colony in Norway to give birth to its pups, we can present the life history of the mother bat including the reproductive data of five more consecutive years. This enabled us also to evaluate the birthing process of the conjoined twin in the light of physiological behavioural birthing data.

Abbreviations: AccA, arteria carotis communis of the autosite; AciP, arteria carotis interna of the parasite; Acl, recurrent artery gaining central lung; AcP, arteria carotis of the parasite; adl, adrenal left; adr, adrenal right; Anf, artery to nuchal brown fat reserve; AoA, aorta of the autosite; Aoc, supplementary artery gaining the third otic capsule; AoP, Aorta of the parasite; ApA, arteria pulmonalis of the autosite; ApcP, arteria pulmonalis of the parasite to central third lung; ApP, arteria pulmonalis of the parasite; AsA, arteria subclavia of the autosite; AsP, arteria subclavia of the parasite; AtA, atrium of the autosite's heart; AtP, atrium of the parasite's heart; AvA, arteria vertebralis of the autosite; C, clavicula; CA, clavicula of the autosite; CP, clavicula of the parasite; cy, cystic structure; DbA, ductus arteriosus botalli of the autosite; DbP, ductus arteriosus botalli of the parasite; es, oesophagus; F, femur; gbl, gall bladder left; gbr, gall bladder right; go, gonads; H, humerus; HeA, heart of the autosite; HeP, heart of the parasite; I, ilium; kil, kidney left; kir, kidney right; kis, kidney single; li, large intestine; liv, liver; mrr, mandibular remnant right; R, radius; rdt, rudimentary digestive tract; rza, right zygomatic arch; SA, scapula of the autosite; Sfu, scapulae fused; si, small intestine; so, sternum ossification center; spl, spleen; st, stomach; TavA, tricuspid aortic valve of the autosite; TavP, tricuspid aortic valve of the parasite; TbP, truncus brachiocephalicus of the parasite, seemingly short junction; tel, testicle left; ter, testicle right; thA, thymus autosite; thP, thymus parasite; Ti, tibia/fibula; TpvA, tricuspid pulmonary valve of the autosite; TpvP, tricuspid pulmonary valve of the parasite; t, t1, t2, trachea; ub, urinary bladder; ur, ureter; url, ureter left; urr, ureter right; ut, urethra; VcA, vena cava of the autosite; VcP, vena cava of the parasite; VjeA, vena jugularis externa of the autosite; VjiA, vena jugularis interna of the autosite; VjP, vena jugularis parasite; vlA, left ventricle of the autosite; Vnf, vein from nuchal fat reserve; Voc, recurrent vein from the third otic capsule; vrA, right ventricle of the autosite; VsA, vena subclavia of the autosite; VsP, vena subclavia of the parasite; *x*, image processing artefact.

1 | Introduction

Twinning is a relatively rare occurring phenomenon in normally uniparous animals and humans. The global twinning rate in humans is actually about 1.2% (Monden et al. 2021). In monotocous animals like cattle, the average rate is about 3%–5%, varying largely in different breeds (Samad 2022). Horses show a comparable average rate of 3.5% in Thoroughbred mares (Wolc et al. 2006). In European bats, twinning is more common as they produce between 1 and 1.9 pups per litter (average litter size of 1.4 pups) depending on the size of the species, their latitudinal distribution, and the pup size at birth (Haarsma and Siepel 2013). The common noctule (*Nyctalus noctula*) was shown to be able to adapt its reproductive strategies of bearing one or two pups as a trade-off between energy expenditure in relation to natural resources and reproductive success (Zukalova et al. 2022). The northern bat (*Eptesicus nilssonii*), the species of concern in this case, most often gives birth to larger single pups in comparison to other similarly sized European bats, enabling the young to be weaned off earlier during the year in order to cope with the short summers in the northern latitudes (Haarsma and Siepel 2013; Fjelldal and van der Kooij 2024).

Twinning results either from simultaneous fertilisation and nidation of two separate ova resulting in dizygotic twins or from the complete splitting of a single fertilised ovum giving rise to a monozygotic twin. If the fission in early embryonic development is either incomplete or a fusion of two early developmental stages occurs, conjoined twins will be produced (Sharma et al. 2010). Conjoined twins might either manifest as symmetrically well-developed twins joined together at one single out of eight distinct regions or as asymmetrical twins. The latter, so-called parasitic or heteropagus twins, are characterised by the presence of one fully developed individual (autosite) with either external or internal supernumerary organs or limbs (Spencer 2001). Similar to the symmetrical twins, the anatomically defective parasitic twin (parasite) is also attached to its well-developed counterpart at the same defined regions (Spencer 2000; Sharma et al. 2010). The spectrum of anatomical defects of the parasite is very diverse. The development of the parasite primarily depends on the more extensively intact autosite. Given the rarity of parasitic conjoined twins, the incidence can only be estimated in humans or larger animal breeding facilities with systematic birth defect registration. A calculated global average prevalence of 1.47 conjoined twins per 100,000 human births is based on nationally available surveillance programmes which show wide variations for different countries (Mutchinick et al. 2011). The incidence of human asymmetrical parasitic twins is estimated to be between 0.02 and 1 per 100,000 births (Sharma et al. 2010). Martínez-Frías et al. (2009) indicate the incidence of symmetrical and asymmetrical conjoined twinning in humans in Spain with 0.7 and 0.04 per 100,000 births, respectively. In larger colonies of laboratory animals, the frequency of conjoined twinning in inbred guinea pig populations ranges from 0.7 to 7 per 100,000 births (Hong et al. 1977). In vitro cultured blastocytes of Swiss Webster mice show the occurrence of spontaneous monozygotic conjoined twinning in one of 2000 blastocytes (Wan et al. 1982), not allowing a differentiation into symmetrical or asymmetrical twins.

Symmetrical and asymmetrical conjoined twinning is well documented in livestock like cattle (Hiraga and Dennis 1993; Schulze et al. 2006) and pigs (Selby et al. 1973; Kulawik et al. 2017) in peccary (Benirkschde et al. 1995) as well as in companion and laboratory animals (Hong et al. 1977; Hynd et al. 2013; Tejmi et al. 2022) or in zoo animals (Kompanje and Hermans 2008; Langer et al. 2014) where births are taking place under controlled conditions. In free ranging non-chiropteran animals this rare phenomenon has been documented in the rat and the hedgehog (Kompanje and Hermans 2008), in sea turtles (Bárcenas-Ibarra et al. 2015) as well as in cetaceans (Kamiya et al. 1981; Kawamura and Kashita 1971; Zinchenko and Ivashin 1987; Dabin et al. 2004; Kompanje 2005). In the latter the defective embryos are mostly found in utero during the dissection of killed pregnant females. Given that most conjoined twins are either stillbirths or non-viable, they become susceptible to scavengers or environmental decay, particularly in the context of free-ranging wild animals, making their discovery a fortuitous event.

Conjoined twinning in the large mammalian order of chiroptera is only reported in three cases of free ranging bats (Peterson and Fenton 1969; Urban et al. 2015; Nogueira et al. 2017). The first described case was a middle-sized insectivorous bat *Eptesicus fuscus* from Canada, the second a small fructivorous bat *Artibeus phaeotis* from Belize and the third a large sized Neotropical phyllostomid fructivorous bat attributed to the *Artibeus* genus from Brazil.

Based on micro-CT scans, we describe the detailed external and internal anatomy of a parasitic conjoined twin of a northern bat (*Eptesicus nilssonii*) found dead several hours post-partum in a nursery colony associated with a bat care centre in Norway. In order to decipher if the twin is of monozygotic or dizygotic origin, a genetic analysis of tissue samples collected from either individual of the twin was performed. The extracted DNA was sequenced for relatedness calculations. Additionally, the life history of the twins' mother is described.

2 | Material and Methods

The parasitic twin described was found dead in the midst of excrements in a bat box in Slattum, Nittedal municipality, Norway. With a forearm length of 9.3 mm (parasite)– 9.8 mm (autosite) and a total birth weight of 1.45 g the twin was below the normal weight (2.4–3.0 g; $n = 6$) and size (forearm 14.2–18.8 mm; $n = 17$) range of cubs which were born at the same location (Fjelldal and van der Kooij 2024).

2.1 | Microscopic Computed Tomography (Micro-CT) Imaging and Anatomical 3D-Reconstruction

All micro-CT scans were acquired using an Xradia MicroXCT-400 (Carl Zeiss X-Ray Microscopy, Pleasanton, CA, USA). The conjoined twin specimen was mounted in a plastic container in 70% ethanol and scanned at 90 kVp/88 μA using the 0.4× detector assembly (isotropic voxel size = 13.02 μm) to reveal the ossified parts of the skeleton. Subsequently, the specimen was dehydrated

to absolute ethanol and stained for 1 week in 1% (w/v) elemental iodine in absolute ethanol (I_2E) to enhance soft tissue contrast (Metscher 2009). After staining, the embryo was washed in absolute ethanol to remove unbound iodine from tissues and mounted in a plastic container again in absolute ethanol. The I_2E-stained conjoined twin was scanned at 100 kVp/80 μA using the 0.4× detector assembly (isotropic voxel size = 10.64 μm) to reveal soft tissue anatomy. In addition, a higher magnification interior tomography was acquired for each of the two hearts at 80 kVp/100 μA using the 4× detector assembly (isotropic voxel size = 4.90 μm). For comparison, a physiologically developed *Eptesicus nilssonii* reference specimen of similar body size (born in a wild colony and found dead several days after delivery) was also stained with 1% (w/v) I_2E for 1 week and scanned at 80 kVp/100 μA using the 0.4× detector assembly (isotropic voxel size = 23.69 μm). Virtual slices (tomograms) were reconstructed with the XMReconstructor software supplied with the scanner. Reconstructed tomography volumes were saved in *.TXM format.

Image volumes were imported into the 3D reconstruction software Amira 2022.1 (FEI Visualisation Sciences Group, part of Thermo Fisher Scientific, Mérignac Cédex, FR). The four scans of the conjoined twin (unstained whole body, I_2E-stained whole body, I_2E-stained left heart, I_2E-stained right heart) were registered based on normalised mutual information using the *RegisterImages* tool. The ossified skeleton was segmented using threshold segmentation from the unstained whole-body scan. Internal organs were segmented from the I_2E-stained whole-body scan in the *SegmentationEditor* using different manual segmentation tools. Based on segmentation, surface models were created using the *GenerateSurface* tool. Surface models were processed using several iterations of smoothing and triangle reduction, followed by remeshing. Anatomical reconstructions were limited by image contrast and resolution. Thus, for example, for the vasculature only larger vessels could be identified and reconstructed, while smaller features of the vascular system were often not visible. The same may be true for other organ systems (like the genital system of the parasite), so whenever we state that a feature could not be detected or clarified, this does not necessarily mean that this anatomical feature was absent. Indeed, some features (such as a pancreas) could have been present in the specimen but possibly just could not be unambiguously identified in the present datasets.

2.2 | DNA Extraction and Sequencing

In order to elucidate if the twin is the result of an incomplete fission of a monozygotic embryonic primordium or a fusion of dizygotic early embryonic stages, we used tissue for the DNA extraction that was harvested by severing a toe from the autosite (A100) and the parasite (P100) respectively after the CT scan. The harvested tissues were submitted to The Finnish Museum of Natural History University of Helsinki, Finland for further genetic analysis. DNA was extracted using the QIAamp DNA Micro Kit (Qiagen, Hilden, Germany) and the DNA was stored at −80°C. The sequencing was conducted at Novogene (Cambridge, United Kingdom). Novogene NGS DNA libraries were prepared and run on the Illumina Novaseq 6000 platform to generate 2 × 150 bp reads. P100 was run twice to obtain enough reads. The whole-genome sequencing provided ~80 million reads of sequence data. Adapter sequences were removed from all sequenced reads and trimmed with fastp version 0.21.0 (Chen et al. 2018) with a minimum quality score of 20 and then used as an input for the analysis.

2.3 | Read Alignment and Relatedness Calculation

The reads were aligned to a northern bat genome version mEptNil1.1 (GCA_951640355.1; van der Kooij et al. 2023) using Bowtie2 version 2.4.4 (Langmead and Salzberg 2012) with sensitive-local setting on. Alignments were sorted with Samtools version 1.16.1 (Danecek et al. 2021) and deduplicated with Picard MarkDuplicates version 2.27.5 ("Picard Toolkit." 2019. Broad Institute, GitHub Repository. https://broadinstitute.github.io/picard/; Broad Institute). Due to low quality of the DNA, the single nucleotide polymorphisms (SNPs) were called with two different types of callers and then combined to ensure high accuracy of the genotypes. We used both ANGSD 0.935 (Kim et al. 2011; Korneliussen et al. 2014) and GATK 4.3.3 (Van der Auwera and O'Connor 2020). In ANGSD, we used the following specifications and filters: uniqueOnly 1-remove_bads 1-only_proper_pairs 1-C 50-baq 1-minMapQ 20-minQ 20-minInd 2-doCounts 1-setMinDepth 5-setMaxDepth 100-GL 2-doMajorMinor 1-doMaf 1-SNP_pval 1e-6-doPost 2-doGeno 3-doBcf 1-doGlf 2. In GATK HaplotypeCaller was used first with setting-ERC GVCF and the individual vcfs were combined with GATK's CombineGVCFs tool. The variants were genotyped with GATK GenotypeGVCFs with settings --heterozygosity 0.001 and --stand-call-conf 20 and SNPs selected with GATK SelectVariants with settings --select-type-to-include SNP --restrict-alleles-to BIALLELIC. SNPs were filtered with GATK's VariantFiltration with --filter-expression "QD < 2.0 || FS > 60.0 || MQ < 40.0 || MappingQualityRankSum < −12.5||SOR > 3.00 || ReadPosRankSum > −8.00" --filter-name "snp_filter" and selected from the files with vcftools --remove-filtered-all, version 0.1.16 (Danecek et al. 2011).

The SNPs from both callers were further filtered with vcftools version using --minDP 5 --maxDP 50 and --max-missing 1. In order to select the overlapping SNPs from the files, we used Bedtools intersect version 2.30.0 (Quinlan and Hall 2010) (bedtools intersect -u -a GATK.vcf -b ANGSD.vcf) and kept the overlapping SNPs with vcftools --positions. Finally, the SNPs with differing genotypes within an individual from the overlap set were first detected with vcftools --diff-site-discordance and matching genotypes from both callers within the individual were kept with vcftools --positions. Pairwise relatedness was calculated with vcftools using command --relatedness2 (Manichaikul et al. 2010).

The raw reads are available in the NCBI BioProject database (http://www.ncbi.nlm.nih.gov/bioproject/) under BioProject number PRJNA1107911 and GenBank accession numbers SRR28898236 and SRR28898235.

2.4 | Histology

The conjoined twin was stored in 90% ethanol. A small sample was taken from the cranial mass for tissue identification. The sample was embedded in paraffin wax and 3 μm thick histological sections were stained with Haematoxylin and Eosin using a standard protocol.

2.5 | History of the Mother Bat

The mother bat originates from a northern bat nursery colony which is part of the national rehabilitation centre for bats driven by the Norwegian zoological society and situated in the garden of one of the authors and operated by himself (van der Kooij 2007). The facility contains a flight cage connected to a hibernation room. A heated bat box which is accessible both by non-released bats from inside of the flight cage and by released bats from outside of the cage guarantees a soft release of orphaned bats. The colony was established in 2017, when two previously orphaned bats returned to the release box and gave birth to their pups. Since then, 28 pups have been born with up to six free-ranging reproducing females at the same time. Both pups and mothers are measured regularly (size and weight), and their activity is monitored by video- and infrared surveillance during each season (Fjelldal and van der Kooij 2024).

The mother of the twins named Erika was born on June 26th, 2017, and followed a normal development in comparison to other bats born in the colony. The following year she gave birth to her first own pup, the parasitic twin of this case report. Erika gave birth 30 days after her arrival in the box (normal range 23.6–35.6 days at this location).

The birth of the parasitic twin occurred on 16th June 2018 between 9:00 and 24:00. At 9:00 the mother was separate from the main group, which is quite normal before giving birth. The birth itself was not observed.

Erika had a normal weight development during pregnancy and after pregnancy (measured six times before birth, six times after birth). No post-partum problems like discharge, bleeding or pronounced cleaning behaviour of the mother could be observed. Erika stayed 18 days post parturition in the nursery colony. At that time, it dissolved, and two other mothers left at the same date. Weight loss and weight gain followed a normal scheme (first loss, then gain)(Fjelldal and van der Kooij 2024). As Erika does not consume readily available mealworms in the release box, her food intake was entirely natural and could not be monitored.

Erika returned to the release box the following 5 years (2019–2023) giving birth to 5 pups (3 females and 2 males), which all, except one male that died when 8 days old, reached normal fledgling size and weight, although the male was low in weight at birth (1.5 g). None of the pups returned to the release box after the years of their departure.

3 | Results

3.1 | External Morphology of the Conjoined Twin

On first sight the dead fetus presented as a rather indefinable black package sized 2 cm in length and 1 cm in diameter with readily recognisable feet and claws as well as denuded metacarpal finger bones on the front side (Figure 1A). The backside resembled a physiologically sound newborn bat with the two scapulae and the vertebral column clearly identifiable under the intact skin (Figure 1B).

The fetal conjoined bat has been nourished by a single unpaired placenta and a single umbilical cord which was still attached to the abdominal umbilical opening of the dead fetus (Figure 1A,C). The presence of a penis identified him as a male (Figure 1C).

Moistening of the superficially dried fetus by immersion into physiologic saline allowed to unfold the wings and the delicate flight membranes to unravel the ventral and cranial structures (Figure 1C). The head was marked by the presence of a single eye bulb lacking palpebral structures. The eye bulb was located between the cranial borders of two mirrored opposing pinnae on the right cranial side of the head (Figure 1D). The inversely positioned ventral second pinna was only rudimentally developed. Two additional also mirrored pinnae were discernable on the left side of the head. Cranioventrally at the merging point of the cranial ends of all four pinnae, an undefinable roundish soft tissue mass protruded from the cranial face (Figure 1C,D). This mass was rose in colour and seemingly covered by external skin. Ventral to this protrusion burgeoned an additional flight membrane encompassing two additional fore and pelvic limbs (Figure 1C). As no additional internal skeletal structures were present, the twin was defined as a parasitic conjoined twin composed of the autosite and the parasite. The proximal long bones (humerus and femur) of the parasite were intimately conjoined at the neck and chest of the autosite (Figure 1C). The lower parts of the limbs were readily defined. The feet of the parasite were physiologically sized and formed by analogy to those of the autosite. The metacarpal bones were bare of epidermal cover, and the finger bones were missing. These defects were probably inflicted by the mother during the birthing process. Beside these malformations described, the body of the autosite didn't show any external evidence of further pathological deformities.

3.2 | Micro CT Imaging Results of the Conjoined Twin

3.2.1 | Skeletal Findings

The skull of the autosite was normally developed in the caudal sections (Figure 2A,B). However, maxillar and nasal structures were absent (Figure 2C). The mandibulae consisted of angular fragments in loose connection to the skull (Figures 2B and 3B). Teeth were absent. The internal auditive structures were characterised by the presence of three otic capsules of which two were physiologically developed and positioned at the base of the skull (Figure 2D). One additional otic capsule, visible on the left side of the skull, was adequately sized but lacked a defined cochleal compartmentation (Figures 2E and 3C).

The axial skeleton of the autosite, comprising the vertebral column, ribs and pelvis was consistent with the developmental stage of an analogous newborn (Figure 2F–H). The parasite was lacking vertebral bony structures (Figure 2F–H; I–K of the sole skeleton of the parasite can be found in the Figure S2I–K). The appendicular skeletons of the autosite and the parasite were physiologically developed and showed an internal compartmentation into epiphyseal and diaphyseal segments. Two fused bones of the ileum were the only discernable parts of the parasite's pelvis. Developmental divergences occurred also at the junctional sites between the autosite and

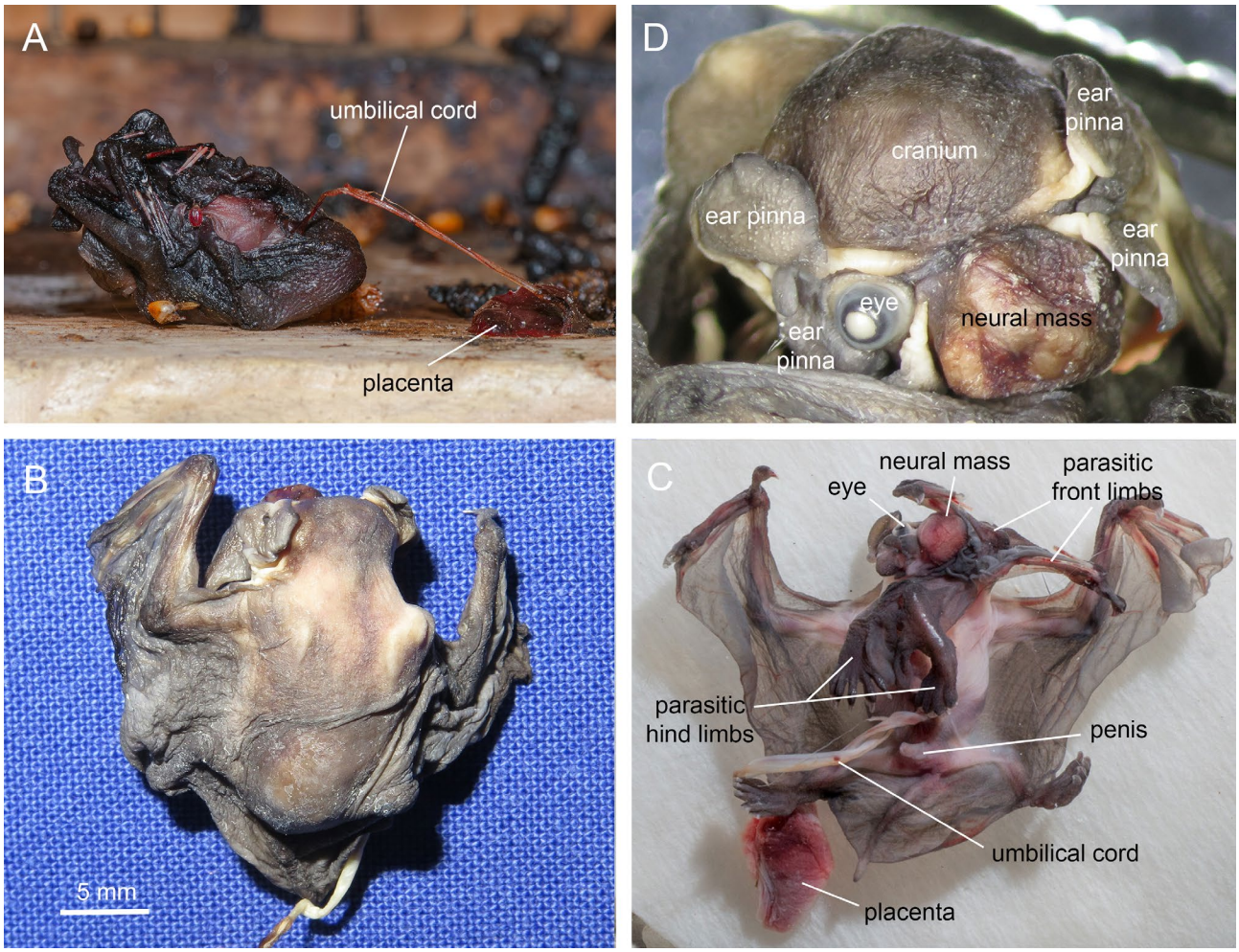

FIGURE 1 | (A) Dead fetus as found on the floor of the breeding box. (B) Dorsal view of the cleaned and unfolded fetus. Both scapulas are clearly visible through the intact skin. (C) Ventral view of the fetus after moistening and unfolding. The well-developed parasitic limbs are attached to the ventral neck and thorax of the autosite. The umbilical cord and the placenta are still attached to the fetus. A neural mass protrudes from the face. (D) Facial view of the fetus. Four opposing ear pinnae are visible. A single eye without palpebral structures is located at the junction of the right pinnae. A neural mass protrudes from the central face between the four pinnae.

the parasite. Both the autosite and parasite show ossifications of the scapulae, claviculae and the processus coracoideus. The sternum in the autosite is paired and failed to fuse ventrally due to the presence of the parasite. It is mostly cartilaginous and only shows two small ossification centres (Figure S2I–K and Figure 8). The connection between the sternal ossification centres is only visible on the regular 2D CT slices but not on the 3D bony reconstruction model. The scapulae of the parasite were fused to form an angulated singular bony structure proximal to and transversely to the paired rudimentary sternal structure (Figure 2F—'Sfu'). The claviculae of both the autosite and the parasite were connected to the paired rudimentary sternum of the autosite.

3.2.2 | Neural System

The central nervous system was composed of a single well-developed spinal cord emerging from the base of the cerebellum and the biventricular brain (Figure 3A). An additional mass of neural tissue that protruded from the face was bare of any bony delimitation (Figure 3B,C). The neural origin of the tissue was verified by a histologic examination of a biopsy (Figure 3D–F). The peripheral nervous system was not studied in further detail.

3.2.3 | Cardiovascular System

Two completely separate hearts were encompassed in the single rib cage and were delimited by the three lungs described below. The bases of the hearts were inclined about 30° to the medial long axis of the twin, whereas the apexes diverged pointing at the opposing sides of the rib cage. The bases of the hearts were interspaced by a third central lung (Figure 4A). The hearts were not mirrored as the ingressions of the venae cavae were located in both hearts on the right side of the fetus. The parasite's heart was mounted by a single atrium. The autosite's heart had two atria, which showed a shunt of both circulations due to an incomplete atrial septation (Figure 4B,C). Two separate ventricles could be discerned on the high-resolution scans of the autosite's heart. As the ventricle cavities were collapsed, a possible shunt between both sides could not be precluded with certainty. The heart of the parasite showed a single venous inflow. The ventricular arrangement of the parasite's heart could

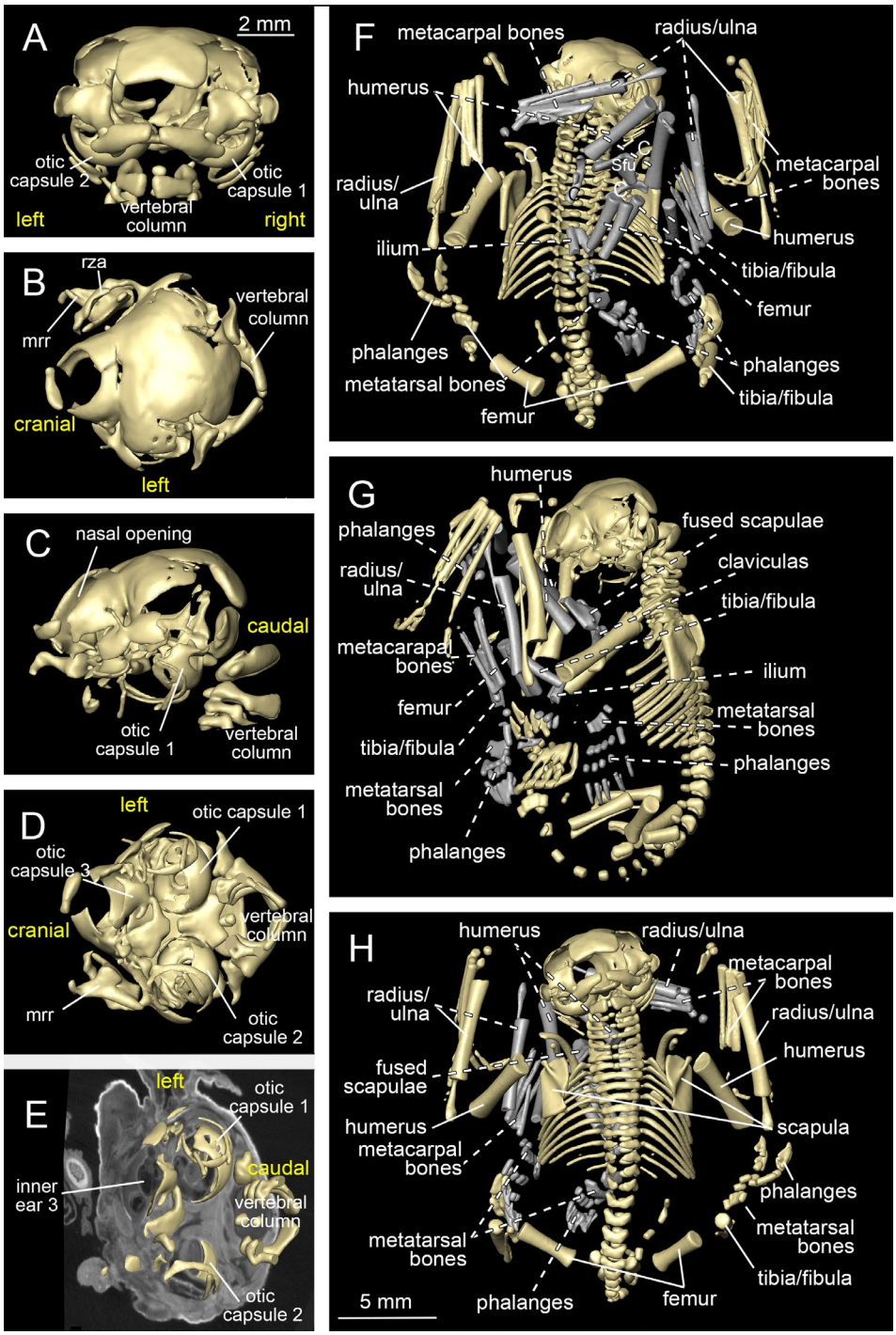

FIGURE 2 | (A–E) Micro-CT 3D reconstructions of the skull, and (F–H) of the whole skeletons. (A) Caudal, (B) dorsal, (C) left lateral and (D) ventral view of the skull. (E) Ventral view of the skull. Composed image of the soft tissues in 2D (grey) and bony structures in 3D (yellowish). Three inner ear structures and their respective capsules are visible. The otic ear capsules 1 and 2 belong to the autosite, the otic capsule 3 originates from the parasite. (F) Ventral, (G) left lateral and (H) dorsal view of the autosite's (yellowish) and the parasite's skeleton (grey). The bones of autosite's skeleton are denoted in continuous lines, those of the parasite in broken lines. 'Sfu' indicates the fused scapulae of the parasite, 'C' the claviculae. Additional images (I–K) of the sole autosite's skeleton can be found in Figure S2.

not be definitively clarified. The main circulatory systems displayed a crisscrossing of arterial outflow and their associated venous returns (Figure 4D). The aorta of the right heart (parasite) turned cranio-medially after exiting the heart and continued in a cranio-distal direction to join the parasite's rudimentary pelvis located on the twin's ventrum and bifurcated into the iliacal vessels. The corresponding venous return directed the blood flow to the left body side into the liver. The exiting liver veins issued into the caudal vena cava of the left heart (autosite). The aorta of the left heart (autosite) emanated in a caudomedial direction to join the pelvis of the autosite. The respective venous reflow was achieved by the caudal vena cava, which caudally contoured the liver on the right body side to discharge into the single atrium of the right heart. A main shortcut between the systems existed

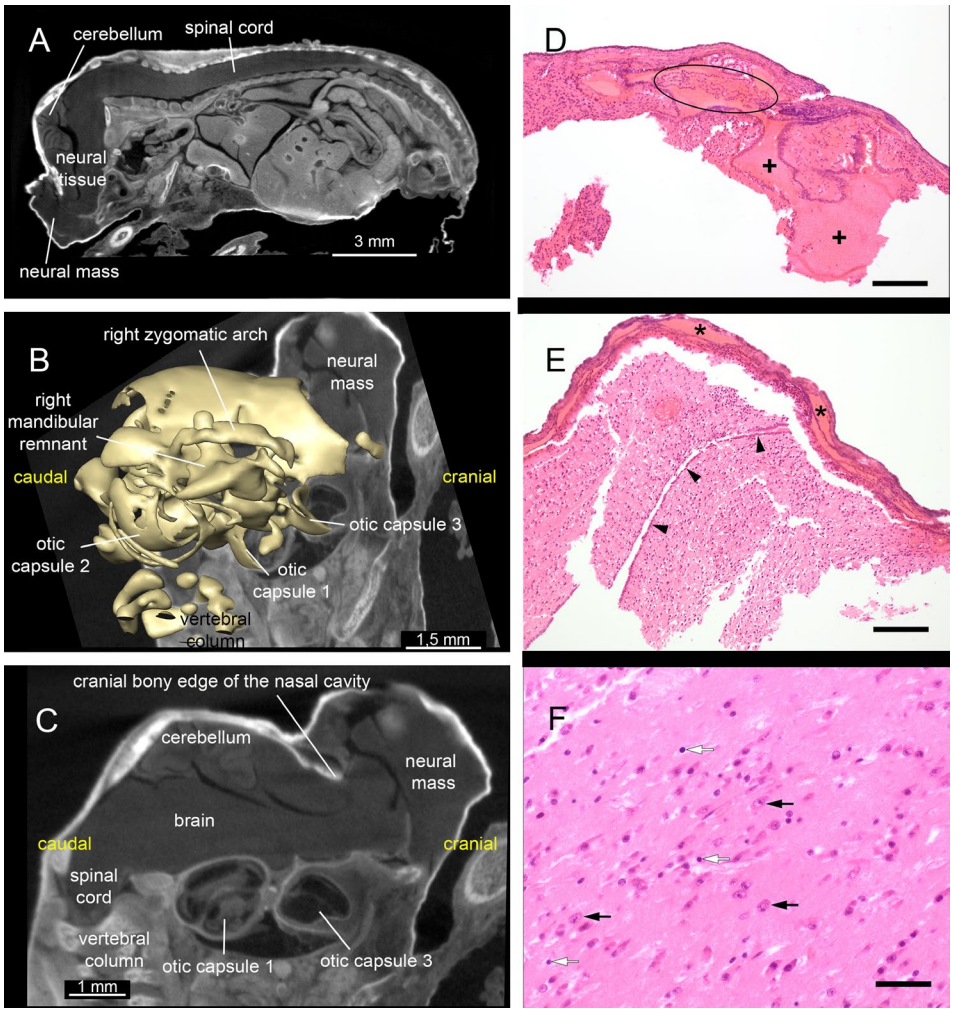

FIGURE 3 | (A) 2D micro-CT image in sagittal median plane of the brain and spinal cord of the twin. (B) Right lateral view of the skull, fused image of 2D soft tissues (grey) showing the protruding neural mass and bony structures (yellowish) in 3D reconstruction. (C) Cross section through the skull. A neural mass connected to the brain is protruding from the nasal cavity and is bare of any bony delimitation. (D–F) Histological pictures from the cranial mass. (D, E) Unstructured neural (brain) tissue is covered by meninges containing irregular and often dilated vessels (*). Arrowheads indicate an abnormal cleft lined by ependymal cells. The meninges blend into a thin dermis and pigmented epidermis on the surface. No osseous structures are present. Haematoxylin–Eosin, Bar = 160 μm. (D) Another area of the same sample. The neural tissue is admixed with irregular spaces (+) that are filled with blood and lined by ependymal cells. A plexus-like structure (encircled) can be seen in the centre. Haematoxylin–Eosin, Bar = 160 μm. (F) Another area of the same sample. The tissue comprises a mixture of larger neurons (black arrows) and smaller glial cells (white arrows). Haematoxylin–Eosin, Bar = 40 μm.

between the truncus brachiocephalicus of the right heart (parasite) and the aorta of the left heart (autosite), crossing over the midline of the twin (Figure 4E). Both aortae and the pulmonary trunks were provided with tricuspid valves (Figure 4F–I). The lungs were bypassed on both sides by a Ductus arteriosus botalli (Figure 4E). The left and the right pulmonary arteries supplied the left and the right lung, respectively (Figure 4J). The central third lung received blood only from the pulmonary artery of the parasite's heart. An additional deviant artery that joined the central third lung originated from a cervical carotid of the parasite (Figure 4E—'acl'). The venous return of the central third lung joined the left and the right heart.

The cervical circulatory system consisted of bilateral common carotid and vertebral arteries originating from the left aortic arch (autosite) and the right brachiocephalic trunc of the left aorta respectively. A supplementary supposably carotid artery leaves the right aortic arch (parasite) after its shunting to the brachiocephalic trunc of the autosite and gains the supplementary otic capsule on the ventral right aspect of the skull (Figure 4K–M). The rudimentary fused pectoral girdle of the parasite featured two presumably additional subclavic arteries originating from the right aortic arch (Figure 4K). The venous cervical reflow is characterised by the presence of three large jugular veins (Figure 4K–M). As previously described in the caudal circulatory anatomy, the venous return from the cervical arteries regains the parasite's heart representing the same cross-over of the cranial circulatory system from the autosite to the parasite.

3.2.4 | Respiratory System

The upper respiratory tract was lacking nasal structures and started at the pharynx with the openings of two entirely

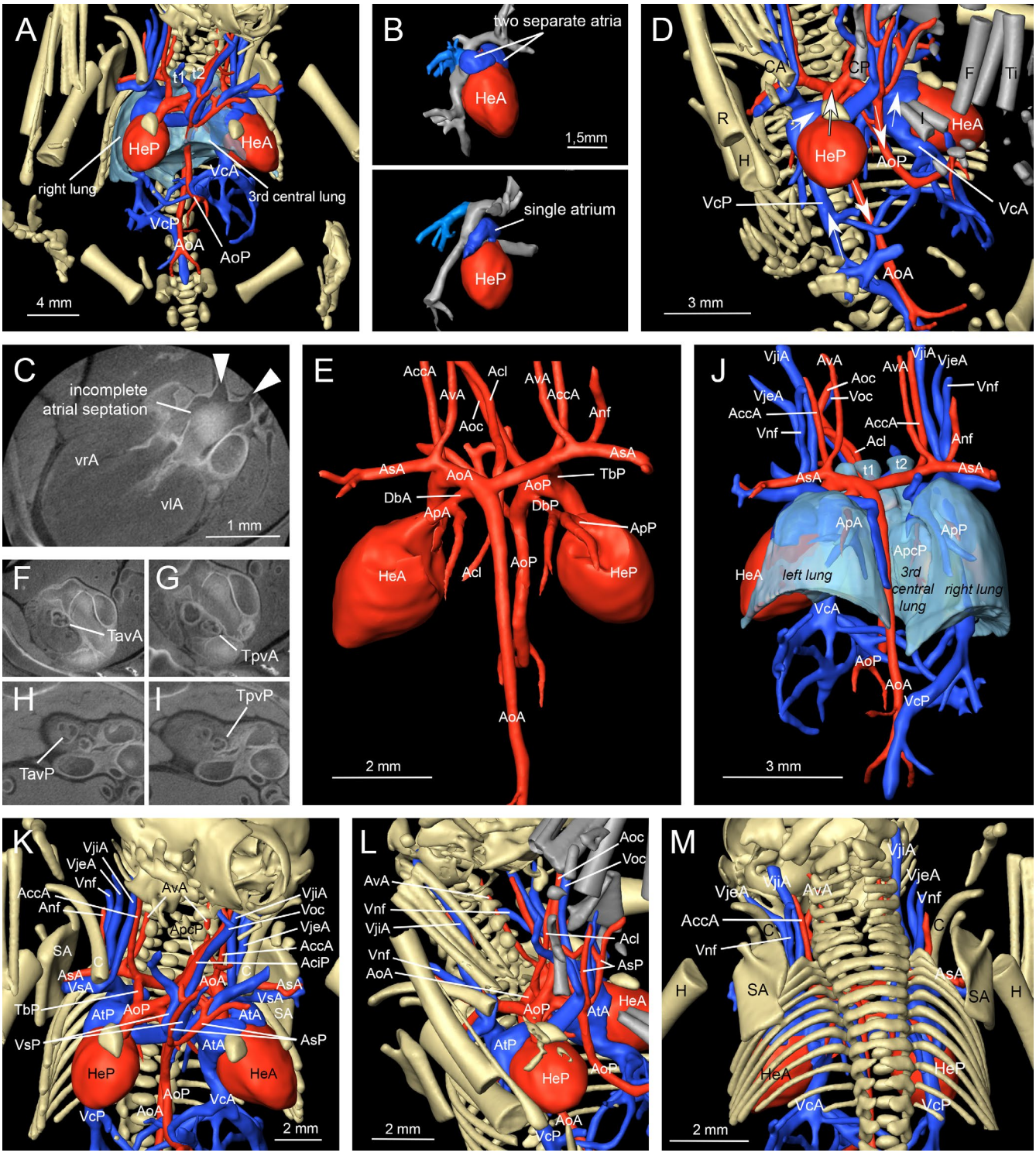

FIGURE 4 | Legend on next page.

separated laryngeal and tracheal structures (Figure 5A). Both tracheas bifurcated into a bronchial system aerating three separate lungs. The scanned reference newborn bat shows a left lung that has a single lobe and a lobulated right lung. A subcompartmentation into several lobes is also visible in the central third lung in conjunction with the aeration of this central lung by a left bronchus from the right trachea as well as the right bronchus of the left trachea (Figure 5B).

3.2.5 | Digestive System

The alimentary tract of the parasite was reduced to a rudimentary blind ending segment of presumably large intestine (Figure 6A). It was not definitely assignable to either small or large intestine. The autosite presented a complete digestive tract compartmentalised into oesophagus, stomach, small and large intestine (Figure 6B). Pancreatic structures were not

FIGURE 4 | (A): Ventral view of a 3D reconstruction of the pulmonary and cardiovascular situation in the body of the autosite. The bony structures of the parasite are omitted for better visualisation. The heart of the autosite and the heart of the parasite are interspaced by a third central lung. The left lung is hidden behind the heart of the autosite. Two tracheas are visible (t1, t2). (B) Demonstration of the two hearts. The heart of the parasite has a single atrium. Circulatory parts of the lung are shown in grey colour. The heart of the autosite is mounted by two atria which show an incomplete septation between themselves (see Figure 4C). (C) High resolution CT of the atria of the heart of the autosite. Both atria communicate through a septal defect. Venous ingression is shown in white arrowheads. (D) Cardiovascular circulatory cross-over (marked with white arrows) between the major vessels of the autosite and the parasite in relation to the skeletal structures of the autosite (yellow) and the parasite (grey). Right ventrolateral view. (E) Hearts and major arterial vessels in dorsal view. The fetal arterial duct of Botalli is physiologically developed for both pulmonal arteries. (DbA, DbP). (F) Base of the autosite's heart showing the tricuspid aortic valve. (G) Base of the autosite's heart showing the tricuspid pulmonary valve. (H) Base of the parasite's heart showing the tricuspid aortic valve. (I): Base of the parasite's heart showing the tricuspid pulmonary valve. (J): Pulmonary and cardiovascular situation in the autosite—dorsal view. The two tracheas are present (t1, t2) Detailed arterial description is already given in (E). (K): Cardiovascular situation in the thorax and the neck of the autosite (skeleton in yellow)– ventral view. Detailed vessel description is given. (L): Cardiovascular situation in the thorax and the neck of the autosite (skeleton in yellow) in relation to the skeletal structures of the parasite (grey). Right lateral oblique view. Not all vessels are labelled. (M): Cardiovascular situation in the thorax and the neck of the autosite (skeleton in yellow)—dorsal view.

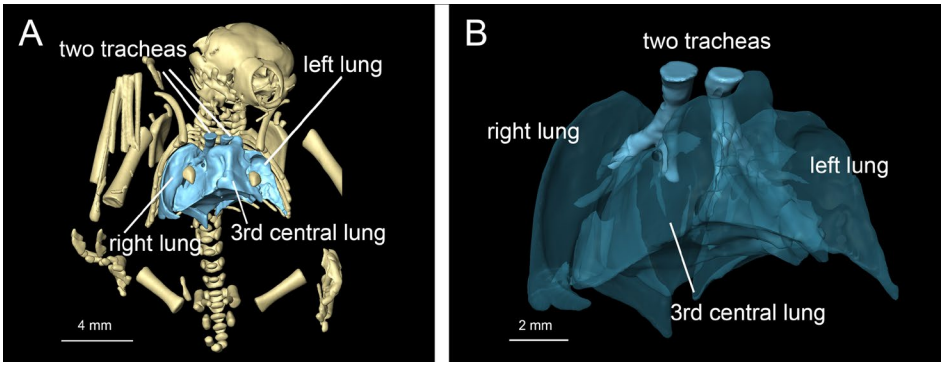

FIGURE 5 | Lower respiratory tract of the autosite. (A) Ventral view of the specimen. Two separate tracheas aerate three distinct lungs. (B) Translucent aspect of the three lungs. Ventral view. The central third lung is aerated by bronchi issuing from both tracheas.

unambiguously discernable. The interactive 3D PDF model features a structure which might be of pancreatic origin (see Figure S1). The stomach of the autosite has a normal axial arrangement with the pylorus exiting on the right side.

The liver consisted of two extended liver lobes on each side of the pagus' abdominal cavity directly ventral to the lungs and the separating diaphragm (Figure 6C,D). Both lobes were fused proximally and showed a shared blood supply. Two distinct gallbladders identifiable through their mucosal internal pattern were present (Figure 6E).

3.2.6 | Urogenital Tract

Both parts of the twin showed an independent urinary system featuring developmental differences. Two fully developed kidneys were located on each side of the vertebral column of the autosite (Figure 7A). The arterial supply originated from the aorta and could be demonstrated on the left side. The arterial supply of the right kidney could not be detected. The adjoined adrenal glands of the autosite could be readily distinguished (Figure 7A,B). The ureters of both kidneys merged into a single urinary bladder in the pelvic region. The bladder voided into a single urethra which ended at the tip of the penis. Two well-developed testicles, epididymides and vas deferens that were connected to the urethra could be demonstrated in the middle of the abdomen, slightly caudal to the kidneys and adjacent to the ureters (Figure 7A,B).

The urinary system of the parasite was only unilaterally developed and consisted of a single kidney with a corresponding ureter which issued into a separate bladder. A cystic structure could be seen on the caudoventral aspect of the parasite's single kidney (Figure 7C). In addition, a short piece of a seemingly rudimentary intestine ended at the base of the parasite's bladder. A cloaca-like unification of bladder and intestine seems to show a single opening; however, the image resolution does not allow to make a definite statement about the exact anatomical situation of the cloaca. The circulatory supply of the parasite's kidney could not be identified. Furthermore, the parasite seems to show a single rudimentary testis and epididymis connected to a vas deferens, as well as a second short rudimentary vas deferens. However, again the limited image resolution does not allow to make a definite statement about the genital organs of the parasite.

The Figure 7D shows the anatomical situs of the abdominal organs of the autosite and the parasite in relation to each other and to the circulatory system in a cranial view.

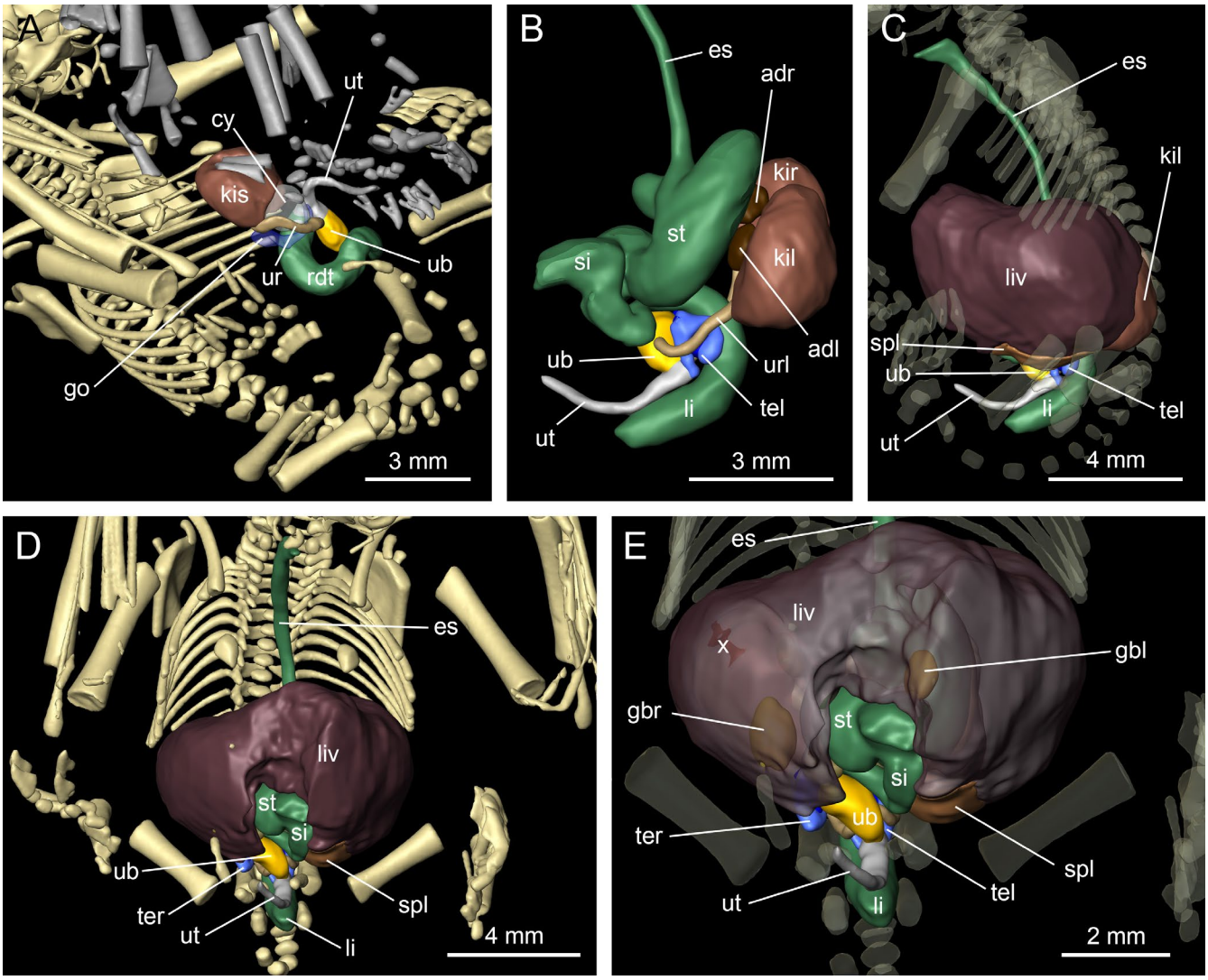

FIGURE 6 | 3D models of the abdominal organs. (A) Right lateral view of the internal abdominal organs of the parasite in relation to the skeletal structures of the autosite (in yellow) and the parasite (in grey). (B) Left lateral view of the isolated abdominal organs of the autosite, the liver and the spleen are omitted for better visualisation. (C) Left lateral view of the abdominal organs of the autosite including the liver and the spleen in relation to its skeletal structures. The skeletal structures are depicted translucently for better visualisation. (D) Ventral view of the abdominal organs of the autosite including the liver and the spleen in relation to its skeletal structures. (E) Ventral view of the abdominal organs of the autosite including the liver and the spleen in relation to its skeletal structures. The liver is depicted translucent in order to show the two existent gall bladders indicating that the liver is composed of the two livers of the autosite and the parasite respectively. A processing artefact (*x*) is present in the right liver lobe.

3.2.7 | Thymus

The cranio dorsal surface of both hearts was most widely covered by the tissues of two separate thymus glands (Figure 8).

3.2.8 | Spleen

A single large spleen could be located on the left ventral border of the conjoined liver in the abdominal cavity of the autosite (Figure 9A,B). The blood supply of the spleen was not visible. Thus, it cannot be excluded that this single spleen is the result of merging of the autosite's and parasite's spleen, as shown in the liver by the presence of two separate gall bladders.

3.3 | Genetic Analysis

All the reads were mapped to the reference genome (Table S1). After calling and overlap filtering, altogether 78,831 SNPs were kept for relatedness calculation (Table S2). The kinship coefficient (ϕ) between the twins was 0.49, which indicates that the bats were monozygotic twins (Manichaikul et al. 2010). Only three SNPs out of 78,831 had different genotypes between A100 (autosite) and P100 (parasite) twins.

4 | Discussion

This case of a conjoined microchiropteran twin is only the fourth report in the order of Chiroptera and the second in a small

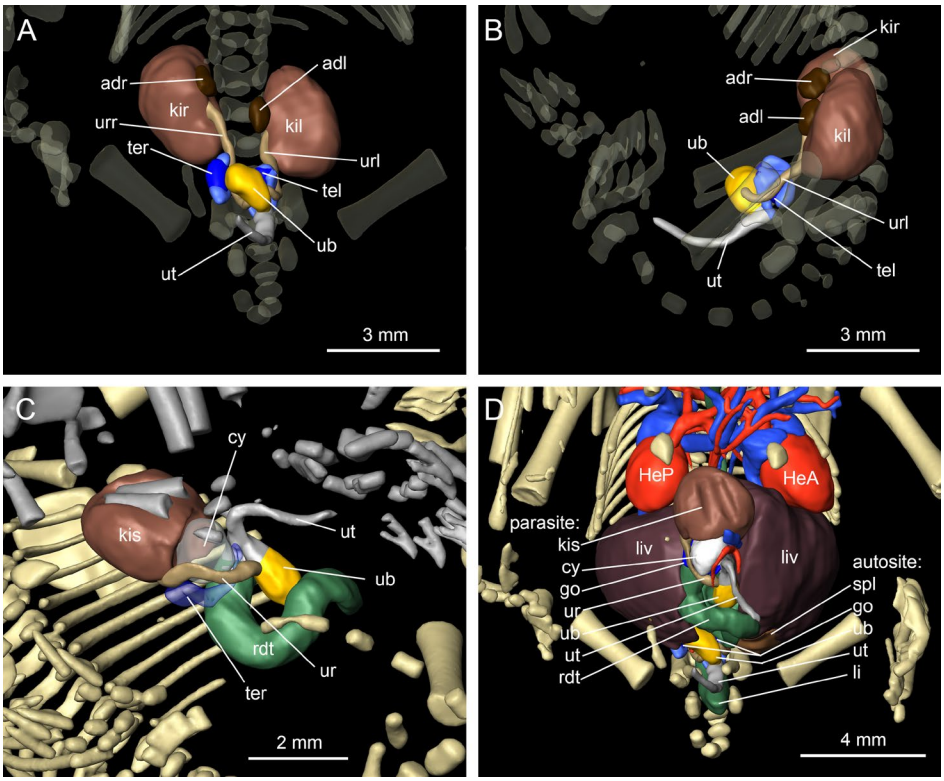

FIGURE 7 | Urogenital organs of the autosite and parasite. Skeletal structures are translucent in A and B for better orientation. (A) Ventral view, and (B) left lateral view of the organs of the parasite. (C) Urogenital organs of the parasite in relation to the parasite's skeletal structures (grey) and the autosite's skeletal structures (in yellow) in right lateral (C) view. (D) Anatomical situs of the abdominal organs of the autosite and the parasite in relation to each other and the cardiovascular as well as the skeletal structures of the autosite in ventral view.

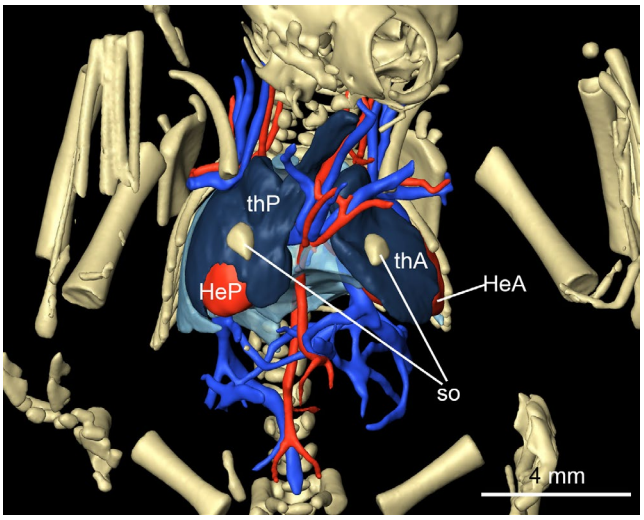

FIGURE 8 | The thymus of the autosite and the parasite in relation to the pulmonary and cardiovascular system in the autosite. Ventral view.

insectivorous bat species, the other two cases being from fructivorous bats (Urban et al. 2015; Nogueira et al. 2017). The cryptic mode of life, their small size and the sparsity of the phenomenon itself make the encounter of a dead born conjoined twin of an insectivorous bat most unlikely. The case presented here is the result of favourable monitoring conditions of the wildlife conservation efforts of a bat rehabilitation station in Norway. Bats in rehab give birth from time to time, but to our knowledge, the birth of a conjoined twin in such facilities has not been published before. A careful search for dead bats beneath open and individual rich roosts on attics, in caves and beneath bat houses is probably most likely to discover the existence of conjoined twins in the wild.

Following the classification criteria for conjoined twins as published by Spencer (2001) a categorisation of the twin in the present case as cephalo-thoracopagus would implicate the existence of two axial skeletons. Being bare of axial skeletal structures besides the rudimentary pelvis characterises the herein described conjoined twin as parasitic cephalothoracopagus. The protrusion of brain tissue devoid of any cephalic bones from the nose of the autosite might categorise the parasite as an opocephalic conjoined twin.

Conjoined twinning is regarded to occur only in monozygotic, monochorionic and monoamniotic twins (Kaufmann 2004). Several theories on the development of conjoined twins, however, are discussed in the scientific community: the fission and the fusion theory and the initial duplication of morphogenetic potent primordia (Boer et al. 2019). According to the fission theory, an unidentifiable stimulus may lead at the primitive streak phase of the embryonic development to the cleavage of Hensen's node and the embryonic axis, leading to the formation of monoamniotic twins. If the stimulus impacts on a more progressed early embryo, the partition of the developing embryo might be incomplete, resulting either in a conjoined or a parasitic twin. Another theoretical explanation of the development of conjoined twins is based on the possibility of early

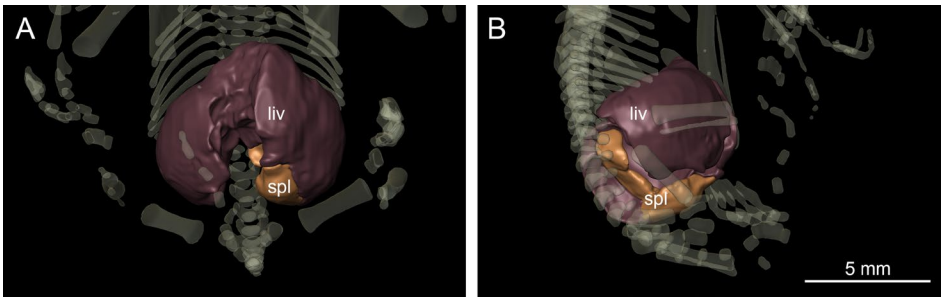

FIGURE 9 | Isolated liver and spleen in relation to the skeletal structures of the autosite. The skeletal structures of the autosite are depicted translucently: (A) ventral and (B) right lateral view.

fusion of two in a first instance dizygotic, monochorionic and monoamniotic embryos. This dizygosity could be genetically proven in a case of a male human baby (Logroño et al. 1997). Besides the fission and fusion theories, the duplication of morphogenetic potent primordia was proposed to be at the basis of the development of conjoined twins (Boer et al. 2019). Our relatedness calculation revealed the present conjoined twin as being of monozygotic origin. Although the DNA was quite fragmented, we used highly conservative SNP calling and filtering settings to avoid including SNP variation due to DNA damage. If the conjoined arrangement of the heteropagus was the result of an initial duplication of primordia or the incomplete cleavage of a primitive streak cannot be ascertained. No genetic data are available on the ratio between monozygotic and dizygotic twins in bat species producing healthy twin births on a regular basis.

The noxious stimulus leading to the formation of conjoined twins in humans may be ingested teratogenic or mitogenic substances although in several studies none of these substances could be linked directly to the occurrence of asymmetric conjoined twinning (Sharma et al. 2010). In small mammals urethan was identified in hamsters to induce a higher number of conjoined twinnings (Ferm 1969). Prochlorpromazine is reported to produce conjoined twins in rats (Roux 1959) and vincristine sulphate, a mitotic inhibitor used in cancer therapy, may induce conjoined twinning in mice (Kaufmann and O'Shea 1978). The revelation of the impetus leading to the conjoinment in free ranging animals like bats is hardly possible. As our conjoined twin is the only Siamese twin amongst 28 births of free ranging bats in the rehabilitation facility during seven seasons, no clear environment or genetic incentives are obvious.

The detailed investigation of the cardiovascular arrangements in this case was triggered by the existence of two fully separated hearts. The axial orientation and the development of internal organs in conjoined twins is influenced by interactions of signalling secretions and their directional flow in the gastrula initiated by a ciliated left–right organiser (Levin et al. 1996; Tisler et al. 2017). Laterality defects resulting from the mutual influence of the developing primitive streaks can only be interpreted with caution in this case. The axial orientation of the hearts in conjunction with their ingressive and egressive vasculature aids in general as a landmark in the localisation of laterality defects. Only the heart of the autosite showed distinctive left and right atria and ventricles respectively even though the atria communicated dorsally. According to Spencer (2001) the absence of a fully functional heart capable of supporting the growth and thriving of the embryo constitutes the etiologic basis of all parasitic twins. The defective heart of the parasite endued with a single atrium concatenated to a singular venous return supports this basic premise. The parasite's cardial ventricular arrangement could not be defined. The aortas of both hearts are exiting the base of the heart and continue in opposite directions. In the reference animal, the aortic arch is directed in a caudomedial direction and follows the course of the vertebral column. In analogy to the reference bat, the aortas of the parasite and the autosite are pursuing the course in the direction of the vertebral columns. The vertebral column of the parasite is nonexistent but could be expected to be localised on the ventral aspect of the autosite based on the localisation of the parasite's single kidney. This would lead to the conclusion that the cardial arrangement with the apexes pointing in opposite directions is not due to laterality defects but simply results from the intertwining development of the thoracic organs of fronting individuals. This premise is further supported by the anatomical compartmentation of the central third lung lobe in the conjoined twin. In the reference animal only, the right lung is lobulated whereas the left lung lobe has a single pulmonary lobe. In the conjoined twin, both outer lungs are not lobulated, characterising them as left lungs. The third central lung shows two defined lobulations resulting presumptively from the fusion of the two right pulmonary lobes of the parasite and the autosite. No laterality defects could be detected in the present conjoined twin.

One spleen could be detected by micro-CT scan in the conjoined abdominal cavities of the twins. The assumption based on clinical observations that the absence of spleens in human conjoined twins might be a hallmark for laterality defects in prenatal diagnostics could not be proven by the systematic radiological evaluation of preserved pathological human specimens (Oostra et al. 2012). This so-called interaction aplasia due to some developmental genetic signalling interaction in conjoined twins facing each other would explain the absence of one spleen, the absence of a kidney, and only rudimentary development of the digestive and urinary tract of the parasite. The absence of one spleen could not be related to laterality defects in this bat either.

A cystic structure educible on the caudoventral aspect of the parasite's single kidney could be resulting from the impaired outflow through the blind ending atretic urethra. Resolution deficits in the CT scans impaired an exact clarification of these erroneous anatomical arrangements.

The developmental stage of the newborn conjoined twin at birth was approximated by the measurement of the whole-body weight and by the forearm length of the newborn in comparison to compiled data of normal offspring of the same species at the same location (Fjelldal and van der Kooij 2024).

It is assumed that the twin fetus was in a late developmental stage concerning morphological characteristics. However, the assessed total weight was below that of normal new born cups and the size of the forearm, a landmark in the evaluation of neonatal development, was much lower than average normal neonatal size range. In comparison to pups ($n = 17$) that were measured at birth or up to 6.5 h after birth the autosite had 58.0% of fully grown normal length and the parasite 55.0%. Northern bats grow very fast. Weight and forearm lengths change within hours. It is therefore important to compare the measurements of the twins with other pups that have been measured shortly after birth. As all internal organs were in a very good condition, we concluded that the conjoined twin showed a reduced development with a maintained viability to the point of birth. Due to the severe cerebral and cardiac deformities in conjunction with vascular and multiple organic deformities the twin was most probably inviable when disrupted from the maternal placental blood supply. The fetus was expelled with the placenta clinging to the umbilical cord. This might be a sign of premature placental disruption initiating the delivery. In general, the umbilical cord is severed by the mother during birth, and the placenta is expelled at a later stage of the birthing process and consecutively eaten (J.v.d.K., pers. obs.). As the placenta remained attached to the fetus via the umbilical cord and was neither severed nor eaten by the mother, one might interpret this as an indication that the fetus showed no viable signs and was subsequently abandoned by the mother shortly after delivery. The birthing process as such has not been observed, but the mother showed a physiologic pre-birth behaviour of separating from the colony to give birth. There was no sign of a premature birth as the elapsed time of 30 days between the arrival of the female in the breeding box and the birthing process was within the regularly observed time frame (Fjelldal and van der Kooij 2024). No signs for a laborious birth like increased discharge, bleeding or an extensive postnatal cleaning behaviour of the mother was observed neither while giving birth to the twin nor in subsequent births.

This study shows that a parasitic conjoined bat may be delivered by normal birthing process without detrimental effects to the mother. The parasitic conjoined twin was non-viable when dislodged from the placental maternal blood supply due to a multitude of neural, cardiac, vascular and organic non-life supporting defects.

Acknowledgements

This research was supported using resources of the VetCore Facility (VetImaging) of the University of Veterinary Medicine Vienna. Open Access funding provided by Veterinarmedizinische Universitat Wien/KEMÖ.

Conflicts of Interest

The authors declare no conflicts of interest.

Data Availability Statement

The data that support the findings of this study are available from the corresponding author upon reasonable request.

References

Bárcenas-Ibarra, A., H. de la Cueva, I. Rojas-Lleonart, et al. 2015. "First Approximation to Congenital Malformation Rates in Embryos and Hatchlings of Sea Turtles." *Birth Defects Research. Part A, Clinical and Molecular Teratology* 103, no. 3: 203–224. https://doi.org/10.1002/bdra.23342.

Benirkschde, K., A. Hagera, and D. K. Edwards 3rd. 1995. "Observations on Neonatal Mortality of the Chacoan Peccary, *Catagonus wagneri*." *Veterinary Pathology* 32: 532–534. https://doi.org/10.1177/030098589503200511.

Boer, L. L., A. N. Schepens-Franke, and R. J. Oostra. 2019. "Two Is a Crowd: On the Enigmatic Etiopathogenesis of Conjoined Twinning." *Clinical Anatomy* 32, no. 5: 722–741. https://doi.org/10.1002/ca.23387.

Chen, S., Y. Zhou, Y. Chen, and J. Gu. 2018. "Fastp: An Ultra-Fast All-In-One FASTQ Preprocessor." *Bioinformatics* 34, no. 17: i884–i890. https://doi.org/10.1093/bioinformatics/bty560.

Dabin, W., C. Cesarini, I. Clemenceau, et al. 2004. "Double-Faced Monster in the Bottlenosed Dolphin (*Tursiops truncatus*) Found in the Mediterranean Sea." *Veterinary Record* 154: 306–308.

Danecek, P., A. Auton, G. Abecasis, et al. 2011. "The Variant Call Format and VCFtools." *Bioinformatics* 27, no. 15: 2156–2158. https://doi.org/10.1093/bioinformatics/btr330.

Danecek, P., J. K. Bonfield, J. Liddle, et al. 2021. "Twelve Years of SAMtools and BCFtools." *GigaScience* 10, no. 2: giab008. https://doi.org/10.1093/gigascience/giab008.

Ferm, V. H. 1969. "Conjoined Twinning in Mammalian Teratology." *Archives of Environmental Health* 19, no. 3: 353–357. https://doi.org/10.1080/00039896.1969.10666856.

Fjelldal, M. A., and J. van der Kooij. 2024. "Individual Variation in Breeding Phenology and Postnatal Development in Northern Bats (*Eptesicus nilssonii*)." *Ecology and Evolution* 14, no. 10: e70324. https://doi.org/10.1002/ece3.70324.

Haarsma, A.-J., and H. Siepel. 2013. "Macro-Evolutionary Trade-offs as the Basis for the Distribution of European Bats." *Animal Biology* 63, no. 4: 451–471. https://doi.org/10.1163/15707563-00002424.

Hiraga, T., and S. M. Dennis. 1993. "Congenital Duplication." *Veterinary Clinics of North America: Food Animal Practice* 9, no. 1: 145–161. https://doi.org/10.1016/s0749-0720(15)30678-2.

Hong, C. C., R. D. Ediger, and S. Djurickovic. 1977. "Conjoined Twins and Opocephaly in Guinea Pigs: 4 Cases of Congenital Malformation." *Laboratory Animals* 1: 189–191.

Hynd, T. E., C. L. Buckley, and S. Lozanoff. 2013. "Case of Cephalothoracopagus Conjoined Twinning in an Embryonic Mouse." *Birth Defects Research. Part A, Clinical and Molecular Teratology* 97: 412–424. https://doi.org/10.1002/bdra.23151.

Kamiya, T., N. Miyazyki, and S. Shiraga. 1981. "First Case of Dicephaly in Odontoceti." *Scientific Reports of the Whales Research Institute* 33: 127–129.

Kaufmann, M. H. 2004. "The Embryology of Conjoined Twins." *Child's Nervous System* 20: 508–525. https://doi.org/10.1007/s00381-004-0985-4.

Kaufmann, M. H., and K. S. O'Shea. 1978. "Induction of Monozygotic Twinning in the Mouse." *Nature* 276: 707–708. https://doi.org/10.1038/276707a0.

Kawamura, A., and K. Kashita. 1971. "A Rare Double Monster of Dolphin *Stenella caeruleoalba*." *Scientific Reports of the Whales Research Institute* 23: 139–140.

Kim, S. Y., K. E. Lohmueller, A. Albrechtsen, et al. 2011. "Estimation of Allele Frequency and Association Mapping Using Next-Generation Sequencing Data." *BMC Bioinformatics* 12: 231. https://doi.org/10.1186/1471-2105-12-231.

Kompanje, E. J. O. 2005. "A Case of Symmetrical Conjoined Twins in a Bottlenose Dolphin *Tursiops truncatus* (Mammalia, Cetacea)." *Deinsea* 11: 147–150.

Kompanje, E. J. O., and J. J. Hermans. 2008. "Cephalopagus Conjoined Twins in a Leopard Cat (*Prionailurus bengalensis*)." *Journal of Wildlife Diseases* 44, no. 1: 177–180. https://doi.org/10.7589/0090-3558-44.1.177.

Korneliussen, T. S., A. Albrechtsen, and R. Nielsen. 2014. "ANGSD: Analysis of Next Generation Sequencing Data." *BMC Bioinformatics* 15: 356. https://doi.org/10.1186/s12859-014-0356-4.

Kulawik, M., K. Pluta, M. Wojnowska, B. Bartyzel, M. Nabzdyk, and D. Bukowska. 2017. "Cephalothoracopagus (Monocephalic Dithoracic) Conjoined Twins in a Pig (*Sus Scrofa f. Domestica*): A Case Report." *Veterinární Medicína* 62, no. 8: 470–477. https://doi.org/10.17221/155/2016-VETMED.

Langer, S., K. Jurczynski, A. Gessler, F.-J. Kaup, M. Bleyer, and K. Mätz-Rensing. 2014. "Ischiopagus Tripus Conjoined Twins in a Western Lowland Gorilla (*Gorilla gorilla*)." *Journal of Comparative Pathology* 150, no. 4: 469–473. https://doi.org/10.1016/j.jcpa.2013.12.002.

Langmead, B., and S. L. Salzberg. 2012. "Fast Gapped-Read Alignment With Bowtie 2." *Nature Methods* 9, no. 4: 357–359. https://doi.org/10.1038/nmeth.1923.

Levin, M., D. J. Roberts, L. B. Holmes, and C. Tabin. 1996. "Laterality Defects in Conjoined Twins." *Nature* 384, no. 6607: 321. https://doi.org/10.1038/384321a0.

Logroño, R., C. Garcia-Lithgow, C. Harris, M. Kent, and L. Meisner. 1997. "Heteropagus Conjoined Twins due to Fusion of Two Embryos: Report and Review." *American Journal of Medical Genetics* 73, no. 3: 239–243.

Manichaikul, A., J. C. Mychaleckyj, S. S. Rich, K. Daly, M. Sale, and W.-M. Chen. 2010. "Robust Relationship Inference in Genome-Wide Association Studies." *Bioinformatics* 26, no. 22: 2867–2873. https://doi.org/10.1093/bioinformatics/btq559.

Martínez-Frías, M. L., E. Bermejo, J. Mendioroz, et al. 2009. "Epidemiological and Clinical Analysis of a Consecutive Series of Conjoined Twins in Spain." *Journal of Pediatric Surgery* 44, no. 4: 811–820. https://doi.org/10.1016/j.jpedsurg.2008.07.002.

Metscher, B. D. 2009. "MicroCT for Comparative Morphology: Simple Staining Methods Allow High-Contrast 3D Imaging of Diverse Non-Mineralized Animal Tissues." *BMC Physiology* 9: 11. https://doi.org/10.1186/1472-6793-9-11.

Monden, C., G. Pison, and J. Smits. 2021. "Twin Peaks: More Twinning in Humans Than Ever Before." *Human Reproduction* 36, no. 6: 1666–1673. https://doi.org/10.1093/humrep/deab029.

Mutchinick, O. M., L. Luna-Muñoz, E. Amar, et al. 2011. "Conjoined Twins: A Worldwide Collaborative Epidemiological Study of the International Clearinghouse for Birth Defects Surveillance and Research." *American Journal of Medical Genetics. Part C, Seminars in Medical Genetics* 157C, no. 4: 274–287. https://doi.org/10.1002/ajmg.c.30321.

Nogueira, M. R., A. Ventura, C. C. P. da Veiga, R. Monteiro, N. L. Pinheiro, and A. L. Peracchi. 2017. "Dicephalic Parapagus Conjoined Twins in a Large Fruit-Eating Bat, Genus Artibeus (*Chiroptera, Phyllostomidae*)." *Anatomia, Histologia, Embryologia* 46, no. 4: 319–324. https://doi.org/10.1111/ahe.12271.

Oostra, R. J., N. Keulen, T. Jansen, and R. R. Van Rijn. 2012. "Absence of the Spleen(s) in Conjoined Twins. A Diagnostic Clue of Laterality Defects? Radiological Study of Historical Specimens." *Pediatric Radiology* 42, no. 6: 653–659. https://doi.org/10.1007/s00247-011-2316-8.

Peterson, R. L., and M. B. Fenton. 1969. "A Record of Siamese Twinning in Bats." *Canadian Journal of Zoology* 47, no. 1: 154.

Quinlan, A. R., and I. M. Hall. 2010. "BEDTools: A Flexible Suite of Utilities for Comparing Genomic Features." *Bioinformatics* 26, no. 6: 841–842. https://doi.org/10.1093/bioinformatics/btq033.

Roux, C. 1959. "Action Teratogène de la Chlorpromazine." *Archives Françaises de Pédiatrie* 16: 968–971.

Samad, M. A. 2022. "Review on the Impact and Consequences of the Occurrence of Multiple Births in Cattle and Goats." *Journal of Veterinary Medical and One Health Research* 4, no. 1: 1–19. https://doi.org/10.36111/jvmohr.2022.4(1).0031.

Schulze, U., R. Koch, M. Köchling, et al. 2006. "Fallbericht: Ein Ungewöhnlicher Fall Eines Monozygoten Thoracopagus Parasiticus Bei Einem Deutschen Holstein Kalb." *Deutsche Tierärztliche Wochenschrift* 113, no. 2: 41–80.

Selby, L. A., A. Khalili, R. W. Stewart, L. D. Edmonds, and C. J. Marienfeld. 1973. "Pathology and Epidemiology of Conjoined Twinning in Swine." *Teratology* 8, no. 1: 1–9. https://doi.org/10.1002/tera.1420080102.

Sharma, G., S. S. Nazarian-Mobin, M. Lypka, and M. Urata. 2010. "Heteropagus (Parasitic) Twins: A Review." *Journal of Pediatric Surgery* 45, no. 12: 2454–2463. https://doi.org/10.1016/j.jpedsurg.2010.07.002.

Spencer, R. 2000. "Theoretical and Analytical Embryology of Conjoined Twins: Part II: Adjustments to Union." *Clinical Anatomy* 13, no. 2: 97–120.

Spencer, R. 2001. "Parasitic Conjoined Twins: External, Internal (Fetuses in Fetu and Teratomas), and Detached (Acardiacs)." *Clinical Anatomy* 14, no. 6: 428–444. https://doi.org/10.1002/ca.1079.

Tejmi, P., V. Navrátil, L. Zabránsky, and M. Soch. 2022. "Conjoined Twins in Guinea Pigs: A Case Report." *Animals* 12, no. 15: 1904. https://doi.org/10.3390/ani12151904.

Tisler, M., T. Thumberger, I. Schneider, A. Schweickert, and M. Blum. 2017. "Leftward Flow Determines Laterality in Conjoined Twins." *Current Biology* 27, no. 4: 543–548. https://doi.org/10.1016/j.cub.2016.12.049.

Urban, D. J., D. W. Sorensen, J. A. Maier, et al. 2015. "Conjoined Twins in a Wild Bat: A Case Report." *Acta Chiropterologica* 17, no. 1: 189–192. https://doi.org/10.3161/15081109ACC2015.17.1.016.

Van der Auwera, G. A., and B. D. O'Connor. 2020. *Genomics in the Cloud: Using Docker, GATK, and WDL in Terra*. 1st ed. O'Reilly Media.

van der Kooij, J. 2007. "The Norwegian Zoological Society's Bat Care Centre—Five Years of Practice." *Fauna* 60, no. 3-4: 183–189.

van der Kooij, J., S. C. Vernes, E. C. Teeling, M. Mai, L. E. Johannessen, and G. Gundersen. 2023. "The Genome Sequence of the Northern Bat, *Eptesicus nilssonii* (Keyserling & Blasius, 1839) [Version 1; Peer Review: 1 Approved]." *Wellcome Open Research* 8: 362. https://doi.org/10.12688/wellcomeopenres.19896.1.

Wan, Y.-J., T.-C. Wu, and I. Damjanov. 1982. "Twinning and Conjoined Placentation in Mice." *Journal of Experimental Zoology* 221, no. 1: 81–86. https://doi.org/10.1002/jez.1402210110.

Wolc, A., A. Bresinska, and T. Szwaczkowski. 2006. "Genetic and Permanent Environmental Variability of Twinning in Thoroughbred Horses Estimated via Three Threshold Models." *Journal of Animal Breeding and Genetics* 123, no. 3: 186–190. https://doi.org/10.1111/j.1439-0388.2006.00575.x.

Zinchenko, V. L., and M. V. Ivashin. 1987. "Siamese Twins of Minke Whales of the Southern Hemisphere." *Scientific Reports of the Whales Research Institute* 38: 165–169.

Zukalova, K., V. Seidlova, V. Piacek, et al. 2022. "One or Two Pups—Optimal Reproductive Strategies Of Common Noctule Females." *BMC Zoology* 7, no. 1: 18. https://doi.org/10.1186/s40850-022-00119-8.

Supporting Information

Additional supporting information can be found online in the Supporting Information section. **Figure S1:** 3D model: interactive 3D PDF model (in high resolution micro-CT) of the conjoined parasitic twin. **Figure S2:** (I–K) Micro-CT 3D reconstructions of the whole autosite's skeleton in cranial, left lateral and dorsal view. The skeleton of the parasite is omitted for better visualisation. **Table S1:** Number of reads sequenced and sequencing depth. **Table S2:** Number of SNPs called between two callers and overlapping SNPs with same genotypes per individual.